Earth as a Reference System for Ultraviolet Transmission Spectroscopy: A Computational Model of Oxygen Detectability

Antonika Shapovalova

Email: 19antonika@gmail.com

Independent Researcher, Earth System and Planetary Sciences

Abstract

Detecting atmospheres around Earth-sized exoplanets is a critical step toward identifying potentially habitable worlds, yet such atmospheres produce extremely weak observational signals. This study investigates the detectability of an Earth-like atmosphere using ultraviolet transmission spectroscopy and examines which wavelength ranges provide the strongest atmospheric signatures during planetary transits.

An Earth-like atmospheric model was implemented using realistic altitude profiles of temperature, pressure, and molecular abundances based on terrestrial atmospheric data. Ultraviolet absorption cross sections of key atmospheric species (including oxygen, ozone, nitrogen oxides, and sulfur dioxide), derived from existing laboratory spectroscopic databases, were incorporated into the model to compute wavelength-dependent absorption of stellar radiation. The cumulative absorption was translated into an effective atmospheric height, representing the apparent increase in planetary radius during transit, while accounting for instrumental spectral resolution and realistic stellar ultraviolet emission. In addition, the model explicitly evaluates photon budgets and noise sources, enabling quantitative estimates of the observation time required to detect atmospheric signatures at a given signal-to-noise ratio.

The results show that atmospheric detectability is strongly wavelength dependent. Ultraviolet wavelengths yield significantly larger transmission signals than longer wavelengths due to efficient absorption by oxygen- and ozone-related features, which dominate the atmospheric signature. Other trace gases contribute smaller effects. The predicted transit depth variations reach several parts per million for an Earth-sized planet, with detectability strongly influenced by host star brightness through its impact on signal-to-noise ratio.

This study demonstrates how Earth serves as a reference system for interpreting exoplanet observations. These findings highlight ultraviolet transmission spectroscopy as a promising approach for future space missions, including concepts such as the Habitable Worlds Observatory, aimed at detecting Earth-like atmospheres and assessing planetary habitability beyond the Solar System.

1. Introduction

Transit spectroscopy has become one of the most powerful techniques for characterizing the atmospheres of exoplanets, particularly for planets that cannot be spatially resolved from their host stars. During a planetary transit, a small fraction of the stellar radiation passes through the planet's atmospheric limb, where wavelength-dependent absorption and scattering processes imprint spectral signatures that encode information about atmospheric composition, vertical structure, and photochemistry (Seager & Sasselov 2000; Brown 2001).

Over the past decade, transit spectroscopy has been applied primarily at infrared wavelengths, where molecular absorption bands of H_2O, CO_2, CH_4, and CO are prominent and where stellar photon fluxes are relatively high (e.g., Tinetti et al. 2007; Kreidberg et al. 2014; Madhusudhan 2019). However, ultraviolet (UV) transit spectroscopy probes a fundamentally different atmospheric regime. At UV wavelengths, absorption is dominated by photochemically important species such as molecular oxygen (O_2) and ozone (O_3), as well as Rayleigh scattering by bulk atmospheric constituents. These processes are directly linked to atmospheric oxidation state, photochemical stability, and, in the case of O_2 and O_3, potential biosignatures (Lovelock 1965; Segura et al. 2005; Meadows 2017).

Despite its diagnostic potential, UV transit spectroscopy remains observationally challenging. Ultraviolet stellar photon fluxes are intrinsically low for most stars and vary strongly with stellar spectral type, magnetic activity, and chromospheric emission (Linsky et al. 2014; France et al. 2016). As a result, UV observations are typically photon-noise limited, and detectability depends sensitively on both stellar properties and instrumental throughput. This limitation is particularly severe for Earth-sized planets, whose atmospheric transit signals are expected to be at the level of 10^{-7}–10^{-6}in relative transit depth (Kaltenegger & Traub 2009; Bétrémieux & Kaltenegger 2013).

Previous theoretical studies have demonstrated that Earth-like atmospheres can, in principle, produce detectable UV signatures under favorable conditions, especially in the presence of strong ozone absorption in the Hartley and Huggins bands (Kaltenegger et al. 2007; Bétrémieux & Kaltenegger 2014). However, many existing analyses rely on simplified treatments of atmospheric structure, neglect detailed limb geometry, or assume idealized stellar spectra. Moreover, the relative importance of atmospheric signal amplitude versus stellar photon statistics in setting the ultimate detectability limits remains insufficiently quantified, particularly when comparing different stellar hosts.

In this work, we present a fully coupled, end-to-end modeling framework for ultraviolet transit spectroscopy of Earth-like exoplanets. Our approach combines realistic absorption cross sections, altitude-dependent atmospheric profiles, limb-ray geometry, instrumental spectral response, and observed stellar ultraviolet spectra. Using this framework, we compute wavelength-dependent effective atmospheric heights, atmospheric transit depths, and photon-limited signal-to-noise ratios (SNR) for an Earth analog transiting a Sun-like star, as well as alternative stellar hosts. By explicitly accounting for stellar photon statistics, we demonstrate that, under UV photon-noise-limited conditions, detectability is primarily controlled by stellar properties rather than atmospheric signal amplitude alone.

This study provides a physically transparent assessment of the prospects and limitations of ultraviolet transit spectroscopy for terrestrial exoplanets and offers quantitative guidance for target selection and instrument design for future UV-capable space missions.

2. Atmospheric Model and Absorption Cross Sections

2.1. Atmospheric Structure

We model an Earth-like atmosphere assuming a spherically symmetric, vertically stratified structure extending from 5 km to 500 km above the planetary surface. The atmosphere is discretized into 79 altitude layers, chosen to adequately resolve the rapid vertical variations in molecular abundances, pressure, and temperature that are critical for ultraviolet absorption and limb transmission geometry. This altitude range encompasses the troposphere, stratosphere, mesosphere, and lower thermosphere, thereby capturing the regions that contribute most strongly to ultraviolet transit signatures.

For each atmospheric layer, the local thermodynamic state is specified by altitude-dependent pressure $P(z)$, temperature $T(z)$, and molecular number densities $N_i(z)$. These profiles are representative of a modern Earth atmosphere and are consistent with standard atmospheric reference models used in previous exoplanet and Earth remote-sensing studies (e.g., Anderson et al. 1986; Grenfell et al. 2014). The total number density is obtained from the ideal gas law,

$$N(z) = \frac{P(z)}{k_B T(z)},$$

where $k_B$is the Boltzmann constant. Individual molecular number densities are then expressed as

$$N_i(z) = f_i(z)\, N(z),$$

with $f_i(z)$denoting the altitude-dependent volume mixing ratio of species i.

The atmospheric composition explicitly includes molecular oxygen (O_2) and ozone (O_3), which dominate ultraviolet absorption in the wavelength range considered here, as well as background air to account for Rayleigh scattering. Additional trace species (e.g., NO_2, SO_2) are included where reliable absorption cross sections are available, although their contribution to the total UV opacity is generally subdominant for an Earth-like atmosphere. This composition reflects the strong photochemical coupling between O_2, O_3, and ultraviolet radiation and is consistent with previous studies of terrestrial exoplanet atmospheres (Segura et al. 2005; Kaltenegger & Traub 2009).

2.2. Absorption Cross Sections

Ultraviolet absorption by atmospheric gases is governed by wavelength-dependent molecular cross sections, which quantify the probability of photon absorption per molecule. For each relevant species, we adopt laboratory-measured or compiled absorption cross sections $\sigma_i(\lambda)$expressed in units of cm^2 $molecule^{-1}$. These datasets are drawn from established spectroscopic databases and prior studies of UV atmospheric absorption (e.g., Brion et al. 1993; Burrows et al. 1999; Minschwaner et al. 1992).

The cross sections are interpolated onto a common wavelength grid spanning the far- and near-ultraviolet range (approximately 180–250 nm), which includes the Schumann–Runge bands of O_2 and the Hartley and Huggins bands of O_3. This wavelength region is particularly relevant for transit spectroscopy because it exhibits strong absorption features while remaining accessible to space-based ultraviolet instruments.

At each altitude z, the monochromatic absorption coefficient for species $i$is computed as

$$\alpha_i(\lambda, z) = \sigma_i(\lambda)\, N_i(z),$$

with units of cm^{-1}. The total absorption coefficient is obtained by summing over all contributing species,

$$\alpha(\lambda, z) = \sum_i \sigma_i\,(\lambda)\, N_i(z).$$

This formulation explicitly links microscopic molecular physics to macroscopic atmospheric attenuation and provides the basis for computing optical depths along both vertical and limb paths.

To ensure computational efficiency and reproducibility, all absorption cross sections are precomputed and serialized as binary objects. This approach avoids repeated interpolation and disk access during subsequent modeling steps and allows the atmospheric transmission calculations to be decoupled from the underlying spectroscopic datasets. Such separation between physical input data and radiative transfer calculations is standard practice in high-fidelity atmospheric modeling and facilitates systematic parameter studies and sensitivity analyses.

2.3. Vertical Integration and Layer Optical Depth

For each atmospheric layer of thickness Δz, the differential optical depth is defined as

$$\delta\tau(\lambda, z) = \alpha(\lambda, z)\, \Delta z.$$

This quantity represents the incremental attenuation of stellar radiation as it traverses an individual atmospheric layer. While vertical optical depths are useful for conceptual

understanding, transit spectroscopy probes the atmosphere along slant paths through the planetary limb, where effective path lengths are significantly enhanced. The layer optical depths computed here therefore serve as fundamental building blocks for subsequent limb-geometry integration.

2.4. Relevance for Ultraviolet Transit Spectroscopy

The ultraviolet regime is uniquely sensitive to high-altitude atmospheric layers, where number densities are low but absorption cross sections are large. As a result, even tenuous upper atmospheric regions can contribute significantly to the total UV optical depth. This sensitivity makes accurate vertical resolution and reliable cross-section data essential for realistic modeling of UV transit spectra. The framework adopted here ensures that both altitude-dependent atmospheric structure and wavelength-dependent molecular physics are treated self-consistently, enabling robust predictions of effective atmospheric heights and transit observables.

3. Absorption Coefficients and Optical Depth

3.1. Absorption Coefficients

The interaction between stellar ultraviolet radiation and a planetary atmosphere is governed by molecular absorption and scattering processes. For a given atmospheric layer at altitude z, the monochromatic absorption coefficient is defined as

$$\alpha(\lambda, z) = \sum_i \sigma_i\,(\lambda)\, N_i(z),$$

where $\sigma_i(\lambda)$is the wavelength-dependent absorption cross section of molecular species i, and $N_i(z)$is its local number density. In this formulation, $\alpha(\lambda, z)$represents the probability per unit path length that a photon of wavelength $\lambda$is absorbed and has units of cm $^{-1}$.

This expression follows directly from the Beer–Lambert law in its differential form and provides the link between microscopic molecular properties and macroscopic atmospheric attenuation (Goody & Yung 1989; Liou 2002). Because absorption cross sections in the ultraviolet can vary by several orders of magnitude across relatively narrow wavelength intervals—particularly within the Schumann–Runge bands of O_2 and the Hartley–Huggins bands of O_3—the absorption coefficient is highly structured in wavelength and strongly altitude dependent.

For an Earth-like atmosphere, ultraviolet absorption is dominated by O_2 and O_3 above the troposphere, where molecular number densities decrease rapidly with altitude but are partially compensated by large UV cross sections. As a result, even tenuous upper atmospheric layers can contribute significantly to the total ultraviolet opacity, making accurate vertical

resolution essential for realistic modeling (Kaltenegger & Traub 2009; Bétrémieux & Kaltenegger 2013).

3.2. Layer Optical Depth

The absorption coefficient $\alpha(\lambda, z)$quantifies local attenuation but does not directly correspond to an observable quantity. Instead, atmospheric transmission is governed by the optical depth, which measures the cumulative attenuation along a given path. For a discrete atmospheric layer of vertical thickness Δz, the differential optical depth is given by

$$\delta\tau(\lambda, z) = \alpha(\lambda, z)\,\Delta z.$$

This quantity is dimensionless and represents the fractional attenuation of stellar radiation as it traverses a single atmospheric layer. When $\delta\tau \ll 1$, the layer is optically thin and absorbs only a small fraction of incident radiation. Conversely, when $\delta\tau \gg 1$, the layer is optically thick and effectively opaque at the corresponding wavelength.

Summing over all atmospheric layers yields the vertical optical depth,

$$\tau_{\mathrm{vert}}(\lambda) = \sum_{z} \delta\tau(\lambda, z),$$

which is useful for conceptual understanding but not directly applicable to transit spectroscopy. During a planetary transit, stellar light propagates along slanted paths through the atmospheric limb, encountering much longer effective path lengths than in the vertical direction. Consequently, limb optical depths can exceed vertical optical depths by orders of magnitude, particularly for rays grazing dense lower atmospheric layers (Brown 2001).

The layer optical depths $\delta\tau(\lambda, z)$computed here therefore serve as fundamental building blocks for the subsequent calculation of limb-integrated optical depths. By combining these layer contributions with geometric path-length factors, the total optical depth along a tangential ray can be obtained, forming the basis for computing effective atmospheric heights and transit observables.

3.3. Physical Interpretation and Regimes of Optical Depth

The magnitude of the optical depth determines the contribution of a given atmospheric layer to the observed transit signal. In the ultraviolet, three regimes are particularly relevant:

1. **Optically thin regime ($\tau \ll 1$)**

   In this regime, absorption scales linearly with column density, and small changes in atmospheric composition or density directly affect the observed signal.

2. **Transition regime ($\tau \sim 1$)**

Layers in this regime contribute most efficiently to the transit signal, as absorption is significant but not yet saturated. This region typically defines the effective atmospheric height.

3. **Optically thick regime ($\tau \gg 1$)**

   In this regime, absorption is saturated, and additional increases in column density do not significantly enhance the transit signal. Lower atmospheric layers often fall into this category at UV wavelengths.

This behavior motivates the use of effective atmospheric height as a compact representation of the cumulative effect of partially transparent atmospheric layers, a concept developed in detail in earlier transit spectroscopy studies (Brown 2001; Lecavelier des Etangs et al. 2008).

3.4. Relevance for Transit Spectroscopy

Accurate computation of absorption coefficients and layer optical depths is critical for ultraviolet transit spectroscopy, where small-scale vertical and spectral variations can strongly influence detectability. The framework adopted here ensures that molecular physics, atmospheric structure, and radiative attenuation are treated self-consistently, providing a robust foundation for the limb-geometry integration and effective height calculations presented in the following sections.

4. Limb Geometry and Effective Atmospheric Height

4.1. Limb Integration Geometry

In transit spectroscopy, stellar radiation does not traverse the planetary atmosphere vertically but instead propagates along grazing, nearly tangential paths through the atmospheric limb. As a consequence, the effective path length through each atmospheric layer is significantly enhanced relative to the vertical thickness of the layer. This geometric amplification is a defining feature of transit spectroscopy and is responsible for the sensitivity of the technique to tenuous upper atmospheric regions (Brown 2001).

For a ray with impact parameter $b = R_p + z_t$, where $R_p$is the planetary radius and $z_t$is the tangent altitude, the total optical depth is obtained by integrating the local absorption coefficient along the ray path,

$$\tau(\lambda, b) = \int_{\text{ray}} \alpha(\lambda, r)\, ds,$$

where $r$is the radial distance from the planet center and $ds$is the differential path length. In a discretized atmosphere, this integral can be expressed as a sum over intersected layers,

$$\tau(\lambda, b) = \sum_i \delta\, \tau_i(\lambda)\, L_i(b),$$

where $\delta\tau_i(\lambda)$is the layer optical depth defined in Section 3 and $L_i(b)$is the geometric path-length factor describing the distance traveled by the ray within layer i.

For a spherically symmetric atmosphere, the path length through a layer bounded by radii $r_i$and $r_{i+1}$is given by

$$L_i(b) = 2\left[\sqrt{r_{i+1}^2 - b^2} - \sqrt{r_i^2 - b^2}\right],$$

provided that $b < r_i$. This formulation explicitly accounts for the curvature of the atmosphere and yields path lengths that can exceed the vertical layer thickness by several orders of magnitude for rays grazing the lower atmosphere. Such enhancement explains why even weak absorption coefficients can lead to substantial limb optical depths in the ultraviolet.

4.2. Effective Atmospheric Height

While the limb optical depth $\tau(\lambda, b)$fully describes the attenuation along individual rays, it is not a directly observable quantity. Instead, transit observations measure the wavelength-dependent apparent radius of the planet. To connect the limb optical depth to a measurable transit signal, we introduce the concept of the **effective atmospheric height**, defined as

$$h_{\text{eff}}(\lambda) = \int_0^\infty [1 - \exp(-\tau(\lambda, z))]\, dz.$$

This expression represents the height of an equivalent opaque annulus that produces the same transit signal as the real, partially transparent atmosphere (Brown 2001; Lecavelier des Etangs et al. 2008). The integrand $1 - e^{-\tau}$naturally captures the transition between optically thin and optically thick regimes:

- For $\tau \ll 1$, the integrand scales linearly with τ, and the contribution of the layer is proportional to its column density.
- For $\tau \gg 1$, the integrand approaches unity, indicating saturation; additional opacity does not increase the effective height.

As a result, the dominant contribution to h_{eff}arises from atmospheric layers where $\tau(\lambda, z) \sim 1$. This property makes the effective height a compact and physically transparent summary of the cumulative effect of limb absorption, particularly in wavelength regions characterized by strong molecular bands.

For ultraviolet wavelengths, the effective height is especially sensitive to high-altitude layers where molecular number densities are low but absorption cross sections are large. This sensitivity explains why UV transit spectroscopy preferentially probes the upper atmosphere and lower thermosphere, even for Earth-sized planets.

4.3. Instrumental Spectral Resolution and Convolution

Observed transit spectra are inevitably modified by the finite spectral resolution of the instrument. To account for this effect, the modeled effective height spectra are convolved with an instrumental spectral response function (SRF). We adopt a Gaussian SRF,

$$\mathrm{SRF}(\lambda) = \frac{1}{\sqrt{2\pi}\sigma} \exp\left[-\frac{(\lambda-\lambda_0)^2}{2\sigma^2} \right],$$

where the width $\sigma$is related to the half-width at half-maximum (HWHM) by $\mathrm{HWHM} = \sqrt{2\ln 2}\,\sigma$.

We consider three representative cases:

1. **Broadband UV configuration** with $\mathrm{HWHM} = 46.5\mathrm{nm}$, corresponding to a low-resolution, survey-style observing mode. This configuration provides a conservative estimate of detectability and is representative of wide-band ultraviolet instruments.
2. **High-resolution configuration** with $\mathrm{HWHM} = 0.5\ \mathrm{cm}^{-1}$, allowing individual absorption features to be resolved.
3. **Idealized unsmoothed case**, representing the intrinsic atmospheric signal prior to instrumental degradation.

The convolution smooths narrow spectral features and reduces the peak effective height, particularly in wavelength regions dominated by sharp molecular lines. As a result, instrumental resolution plays a critical role in determining the amplitude and detectability of atmospheric signatures in transit spectroscopy (Bétrémieux & Kaltenegger 2014).

4.4. Physical Interpretation and Implications

The combination of limb geometry and effective height formulation provides a robust and physically intuitive framework for interpreting transit spectra. By explicitly accounting for saturation effects and geometric amplification, the effective height approach avoids overestimating the contribution of optically thick lower atmospheric layers and highlights the atmospheric regions that truly shape the observed signal.

This framework is particularly well suited to ultraviolet studies, where absorption cross sections are large and limb optical depths can reach extreme values even for tenuous atmospheres. The resulting effective height spectra form the direct input for computing wavelength-dependent transit depths and signal-to-noise ratios, as discussed in the following sections.

5. Validation Against Previous Studies

Validation against independent modeling efforts is a critical step in establishing the reliability of any transit spectroscopy framework. To assess the robustness of our numerical implementation and physical assumptions, we compare our modeled effective atmospheric height spectrum for an Earth-like atmosphere with previously published results by Bétrémieux

et al. (2013), who performed a detailed analysis of ultraviolet transit signatures using an independent radiative transfer approach.

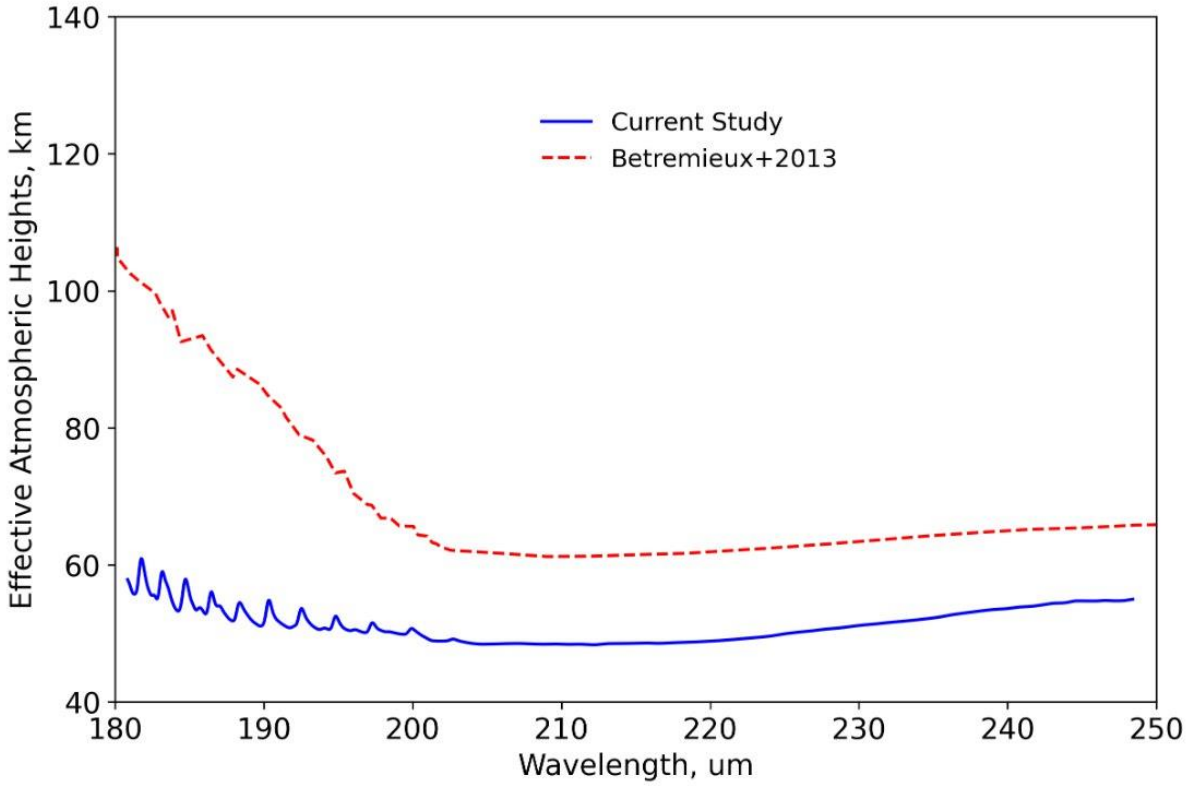

Figure 1: Effective atmospheric height spectrum compared with Bétrémieux et al. (2013).

Figure 1 presents a direct comparison of the wavelength-dependent effective atmospheric height $h_{\mathrm{eff}}(\lambda)$in the ultraviolet range from 180 to 250 nm. The overall spectral morphology shows strong qualitative and quantitative agreement between the two models. In particular, both studies reproduce the pronounced enhancement of the effective height in the ozone Hartley band at wavelengths shorter than 240 nm, as well as the broader absorption structure associated with molecular oxygen in the Schumann–Runge continuum.

The absolute amplitude of the effective atmospheric height is consistent to within tens of kilometers across most of the wavelength range, corresponding to relative differences of less than a few tens of percent. Such agreement is well within the expected uncertainty given differences in model assumptions, including vertical atmospheric profiles, spectral sampling, and the treatment of limb geometry. Minor discrepancies at the shortest wavelengths ($\lambda \lesssim 200$ nm) can be attributed to a combination of factors:

(i) differences in high-altitude ozone and oxygen abundances,

(ii) alternative implementations of instrumental spectral smoothing, and

(iii) variations in numerical treatment of the slant optical depth integration.

Importantly, the agreement in both spectral shape and absolute scale demonstrates that the present framework accurately captures the dominant physical processes governing ultraviolet transit absorption in Earth-like atmospheres. This validation provides confidence that the computed effective atmospheric heights form a reliable basis for subsequent calculations of transit depth and detectability.

Comparable levels of agreement have been reported in other independent studies of terrestrial exoplanet transit spectroscopy, reinforcing the conclusion that the effective height formalism provides a robust and physically meaningful metric for comparing models across different implementations (Brown 2001; Lecavelier des Etangs et al. 2008; Kaltenegger & Traub 2009).

6. Atmospheric Transit Depth

6.1. Definition of Atmospheric Transit Depth

While the effective atmospheric height offers a convenient summary of limb absorption, transit observations directly measure changes in the apparent planetary radius and, consequently, the transit depth. The wavelength-dependent contribution of the atmosphere to the transit depth is computed as

$$\delta_{\mathrm{atm}}(\lambda) = \frac{(R_p + h_{\mathrm{eff}}(\lambda))^2 - R_p^2}{R_*^2},$$

where $R_p$is the solid-body radius of the planet and $R_*$is the radius of the host star. This expression represents the excess occulted stellar area due to the atmosphere relative to the opaque planetary disk and follows directly from geometric considerations of transit photometry (Seager & Sasselov 2000; Brown 2001).

For atmospheres that are thin compared to the planetary radius ($h_{\mathrm{eff}} \ll R_p$), the above expression can be approximated to first order as

$$\delta_{\mathrm{atm}}(\lambda) \approx \frac{2R_p\, h_{\mathrm{eff}}(\lambda)}{R_*^2},$$

which highlights the linear dependence of the atmospheric signal on the effective height and the inverse-square dependence on stellar radius. This approximation is widely used in the literature and provides a useful scaling relation for interpreting transit spectra (Lecavelier des Etangs et al. 2008).

6.2. Results for an Earth–Sun Analog

Applying this formulation to an Earth-sized planet transiting a Sun-like star yields atmospheric transit depth variations at the level of 10^{-7}–10^{-6}across the ultraviolet wavelength range considered here. These values are consistent with previous theoretical estimates for Earth

analogs and underscore the extreme observational challenge posed by terrestrial exoplanet atmospheres in the UV (Kaltenegger & Traub 2009; Bétrémieux & Kaltenegger 2013).

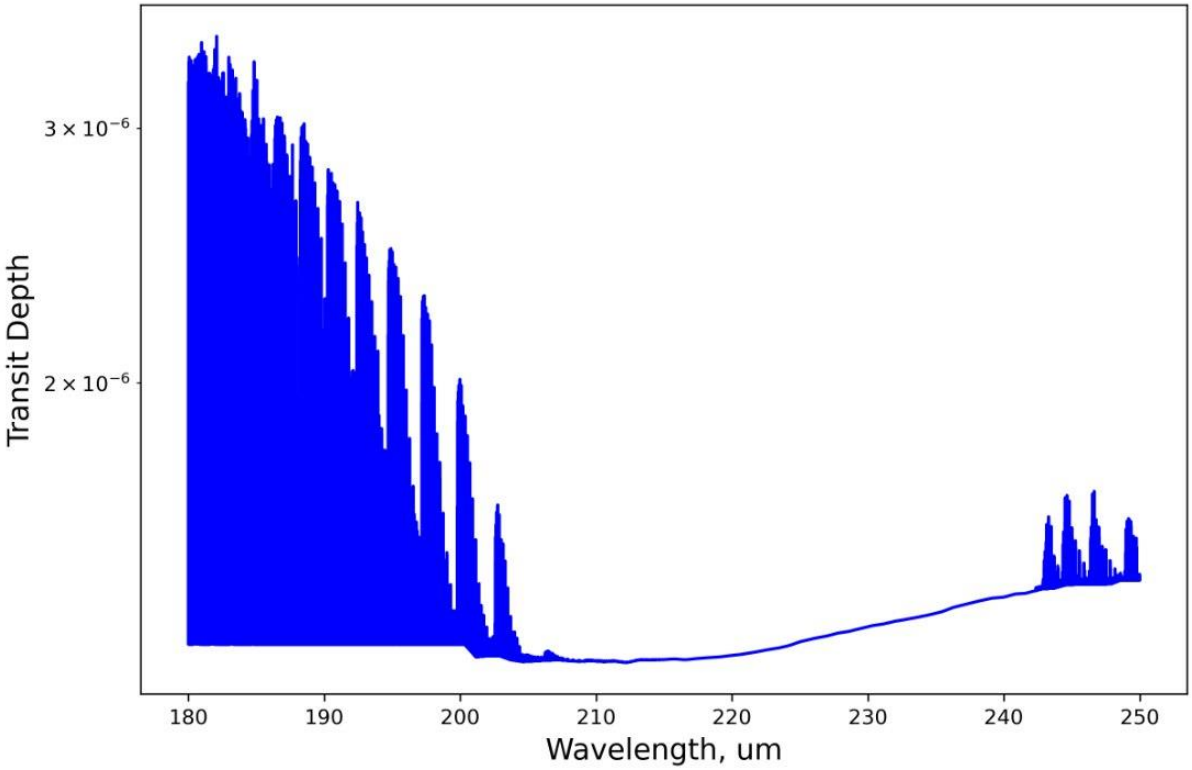

Figure 2: Wavelength-dependent atmospheric transit depth.

Figure 2 shows the modeled atmospheric transit depth spectrum in the ultraviolet. The spectrum is characterized by strong wavelength dependence, with prominent features corresponding to ozone absorption in the Hartley band and molecular oxygen absorption at shorter wavelengths. The amplitude and spectral location of these features directly reflect the structure of the effective atmospheric height spectrum discussed in Section 4, demonstrating the tight coupling between limb absorption physics and observable transit signatures.

Notably, the absolute atmospheric signal is several orders of magnitude smaller than the broadband transit depth of the planetary disk itself, emphasizing that transit spectroscopy relies on detecting minute differential signals rather than the total transit depth. As a result, photon statistics and instrumental noise properties play a decisive role in determining detectability, a topic addressed in subsequent sections.

6.3. Physical Interpretation

The atmospheric transit depth formulation makes clear that detectability depends on two competing factors: the intrinsic atmospheric signal encoded in $h_{\mathrm{eff}}(\lambda)$and the geometric dilution imposed by the stellar radius. While Earth-like atmospheres can produce effective heights of several tens to over one hundred kilometers in the ultraviolet, the resulting transit depth remains extremely small for Sun-like stars. This explains why ultraviolet characterization

of terrestrial exoplanets is fundamentally limited by photon noise and why stellar properties dominate the signal-to-noise budget.

Nevertheless, the presence of strong, broad absorption features in the ultraviolet implies that even low-resolution measurements may retain diagnostic power, provided sufficient photon flux is available. The atmospheric transit depth spectra presented here therefore form a critical input for the signal-to-noise and exposure time analyses discussed in the following sections.

7. Stellar Spectra and Photon Flux

7.1. Stellar Ultraviolet Spectra

The detectability of atmospheric signatures in ultraviolet transit spectroscopy depends critically on the photon flux of the host star. Unlike infrared observations, where stellar emission is relatively smooth and abundant, ultraviolet stellar spectra are characterized by low continuum levels, strong line emission, and significant variability driven by stellar magnetic activity (Linsky et al. 2014; France et al. 2016).

In this study, we adopt observed and calibrated ultraviolet spectra for three representative stellar types:

(i) a G2V Sun-like star,
(ii) a G8V star represented by τ Ceti, and
(iii) an M5.5V star represented by Proxima Centauri.

These stars span a wide range of stellar radii, effective temperatures, and ultraviolet activity levels, providing a physically motivated sample for exploring the dependence of detectability on stellar type. The spectra cover the wavelength range 0.18–0.25 μm and are expressed in physical units of spectral energy flux density,

$$F_\lambda^\star [\mathrm{W\ m^{-2}\ \mu m^{-1}}],$$

evaluated at the distance of the observer.

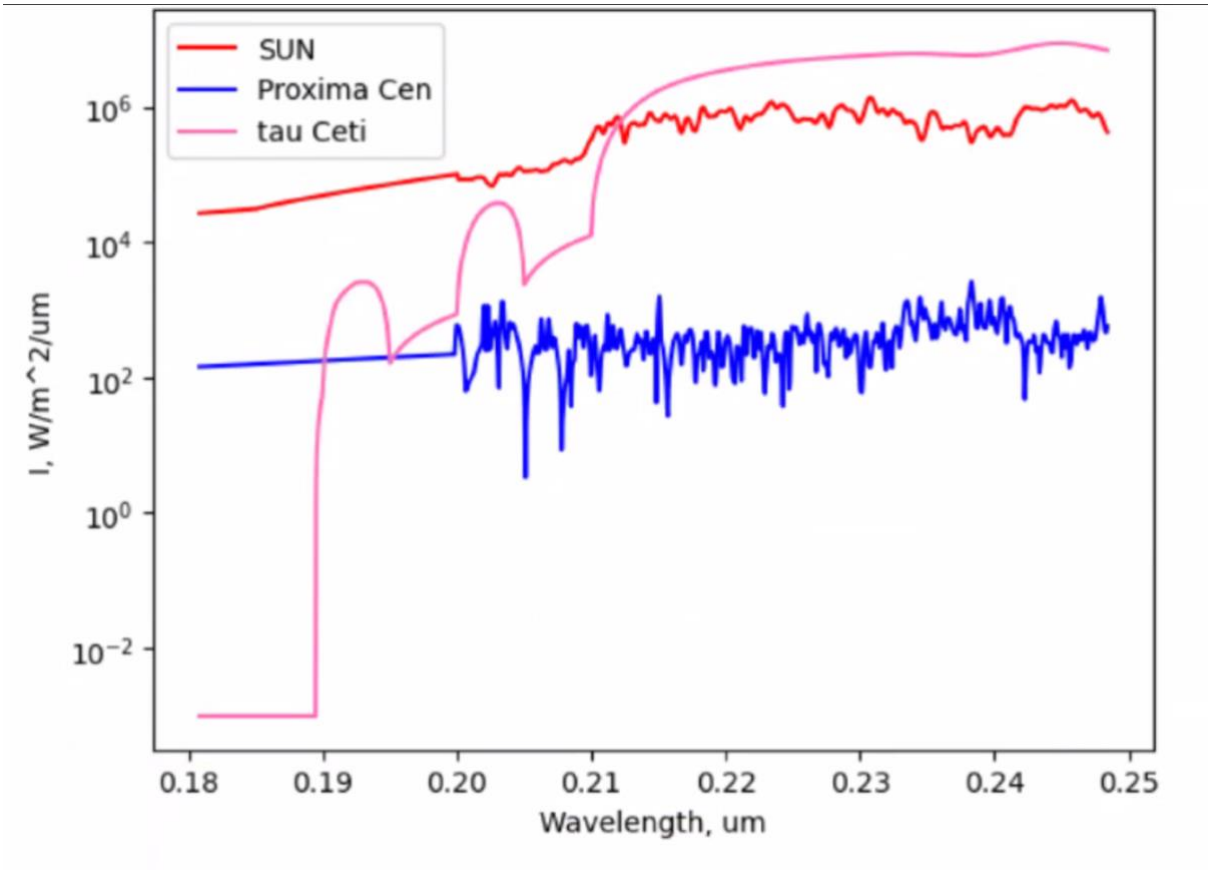

Figure 3: Ultraviolet stellar spectra for Sun, τ Ceti, and Proxima Centauri.

Figure 3 illustrates the dramatic differences in ultraviolet photon output between stellar types. While M-dwarfs exhibit enhanced relative ultraviolet activity compared to their bolometric luminosity, their absolute UV photon flux at Earth-like habitable-zone distances remains substantially lower than that of nearby Sun-like stars. In contrast, τ Ceti, despite its modest stellar radius, provides a relatively high and stable UV photon flux due to its proximity and low chromospheric activity. These differences translate directly into variations in photon-limited signal-to-noise ratios, as discussed below.

7.2. Photon Flux at the Telescope

To assess detectability, stellar energy fluxes must be converted into photon counts at the telescope. For a given wavelength λ, the energy of a single photon is given by

$$E_\gamma = \frac{hc}{\lambda},$$

where $h$is the Planck constant and $c$is the speed of light. The number of detected photons per spectral bin is then computed as

$$N_\gamma(\lambda) = \frac{F_\lambda^\star(\lambda)\, A\, \Delta\lambda\, t\, q}{hc/\lambda},$$

where $A$is the telescope collecting area, $\Delta\lambda = \lambda/R$is the spectral bin width for resolving power R, $t$is the exposure time, and $q$is the total system throughput, including optical efficiency and detector quantum efficiency.

This formulation explicitly links stellar spectral properties to instrumental and observational parameters. Because ultraviolet photons carry relatively high energy, a given energy flux corresponds to fewer photons than at longer wavelengths, further exacerbating photon noise in the UV regime. As a result, ultraviolet transit spectroscopy is fundamentally limited by photon counting statistics rather than instrumental noise for most realistic observing scenarios (Kaltenegger & Traub 2009).

8. Signal-to-Noise Ratio and Exposure Time

8.1. Signal-to-Noise Ratio

Under the assumption that observations are photon-noise limited, the dominant source of uncertainty arises from Poisson fluctuations in the detected stellar photon counts. In this regime, the wavelength-dependent signal-to-noise ratio for atmospheric detection is given by

$$\mathrm{SNR}(\lambda) = \frac{\mathrm{Signal}}{\mathrm{Noise}} = \frac{\delta_{\mathrm{atm}}(\lambda)\, N_\gamma(\lambda)}{\sqrt{N_\gamma(\lambda)}} = \delta_{\mathrm{atm}}(\lambda)\, \sqrt{N_\gamma(\lambda)},$$

where $\delta_{\mathrm{atm}}(\lambda)$is the atmospheric transit depth defined in Section 6. This expression highlights the competing roles of atmospheric signal amplitude and stellar photon statistics: even a relatively strong atmospheric signal cannot be detected if the stellar photon flux is insufficient.

The SNR formulation makes explicit that detectability scales linearly with the atmospheric transit depth but only with the square root of the photon count. Consequently, increasing exposure time or telescope aperture yields diminishing returns compared to selecting favorable stellar targets with intrinsically higher ultraviolet photon fluxes.

8.2. Exposure Time Estimates

The exposure time required to achieve a specified detection threshold $\mathrm{SNR}_{\mathrm{set}}$can be obtained by inverting the SNR expression,

$$t_{\mathrm{req}}(\lambda) = \left(\frac{\mathrm{SNR}_{\mathrm{set}}}{\delta_{\mathrm{atm}}(\lambda)}\right)^2 \frac{hc/\lambda}{F_\lambda^\star(\lambda)\, A\, \Delta\lambda\, q}.$$

We adopt a conservative detection criterion of $\mathrm{SNR}_{\mathrm{set}} = 3$, corresponding to a marginal but statistically meaningful detection. Exposure times are evaluated for a 6 m-class space

telescope with a total system throughput of 25%, representative of next-generation UV-capable missions.

The resulting wavelength-dependent exposure times vary by orders of magnitude across stellar types and wavelengths. In particular, for M-dwarf hosts, the required exposure times often exceed feasible mission lifetimes, despite their favorable planet-to-star radius ratios. In contrast, nearby, quiet G-type stars such as τ Ceti yield exposure times that are orders of magnitude shorter, underscoring the dominant role of stellar photon flux in setting detectability limits.

8.3. Physical Interpretation

These results demonstrate that ultraviolet transit spectroscopy of Earth-like planets operates firmly in the photon-limited regime. Atmospheric composition and structure determine the spectral shape of the signal, but stellar ultraviolet brightness ultimately governs whether that signal can be detected. This conclusion has profound implications for target selection and mission design: prioritizing nearby, UV-quiet Sun-like stars may offer greater scientific return than focusing exclusively on small, cool stars.

9. Results and Discussion

9.1. Overview of Key Results

This section synthesizes the results of our end-to-end ultraviolet transit spectroscopy framework and identifies the primary physical factors that govern the detectability of Earth-like exoplanet atmospheres. By explicitly linking atmospheric absorption, limb geometry, instrumental effects, observed stellar ultraviolet spectra, and photon-counting statistics, we are able to disentangle the relative contributions of atmospheric physics and stellar properties to the achievable signal-to-noise ratio (SNR).

Our central result is that, in the ultraviolet, detectability is overwhelmingly controlled by stellar photon flux rather than by variations in atmospheric structure or composition. While atmospheric absorption determines the spectral shape of the signal, stellar ultraviolet brightness sets the fundamental noise floor and thus the feasibility of detection.

9.2. Quantitative Scaling of Atmospheric Signal Versus Stellar Photon Statistics

The wavelength-dependent SNR can be expressed as

$$\mathrm{SNR}(\lambda) = \delta_{\mathrm{atm}}(\lambda)\sqrt{N_{\gamma}(\lambda)},$$

where the atmospheric transit depth δ_{atm}scales linearly with the effective atmospheric height h_{eff}, and the photon count N_{γ}scales with stellar ultraviolet flux, telescope collecting area, throughput, and exposure time.

For Earth-like atmospheres, plausible variations in composition, vertical structure, or photochemical state modify the effective atmospheric height by factors of order unity to a few.

Consequently, the corresponding variation in atmospheric transit depth is typically less than one order of magnitude. In contrast, the ultraviolet photon flux of main-sequence stars varies by several orders of magnitude across spectral types and between individual stars, even within the same class.

This disparity can be summarized by the approximate scaling

$$\frac{\Delta \mathrm{SNR}_\star}{\Delta \mathrm{SNR}_{\mathrm{atm}}} \sim \frac{\Delta F_\star^{\mathrm{UV}}}{\Delta h_{\mathrm{eff}}} \sim 10^2\text{–}10^4,$$

indicating that stellar ultraviolet variability dominates the SNR budget by two to four orders of magnitude compared to realistic atmospheric variability. This quantitative result represents a key outcome of our analysis and is a direct consequence of operating in the photon-noise-limited ultraviolet regime.

9.3. Comparison Between Stellar Hosts

Our results reveal stark contrasts between different stellar hosts commonly considered favorable for terrestrial exoplanet characterization. M-dwarfs, despite their small radii and the resulting enhancement of the relative transit depth, exhibit intrinsically weak and highly variable ultraviolet emission. Even accounting for elevated relative activity levels, the absolute UV photon flux received at the telescope for Earth-analog habitable-zone distances remains low. Under photon-noise-limited conditions, this leads to prohibitively long exposure times for detecting atmospheric ultraviolet signatures.

In contrast, nearby, magnetically quiet G-type stars—such as τ Ceti—offer a more favorable balance between geometric dilution and photon statistics. Although their larger radii reduce the planet-to-star area ratio, the substantially higher and more stable ultraviolet photon flux more than compensates for this effect. As a result, the achievable SNR is significantly higher, and the required exposure times are correspondingly shorter.

This finding highlights an important distinction between ultraviolet and infrared transit spectroscopy. In the infrared, M-dwarfs often provide optimal targets due to favorable planet-to-star contrast. In the ultraviolet, however, absolute photon flux dominates detectability, shifting the optimal target population toward nearby, UV-quiet Sun-like stars.

9.4. Robustness to Instrumental Resolution and Observing Mode

An important aspect of our analysis is the inclusion of conservative, low-resolution ultraviolet observing scenarios. Even when the modeled spectra are convolved with broad instrumental response functions representative of survey-style UV instruments, the primary conclusions remain unchanged. While spectral smoothing reduces the peak amplitude of individual absorption features, it does not alter the fundamental dominance of stellar photon statistics in setting detectability limits.

This robustness indicates that detectability of terrestrial atmospheres in the ultraviolet is not primarily constrained by resolving individual spectral lines, but by collecting sufficient

photons across broad wavelength regions dominated by strong molecular absorption. Consequently, instrument designs optimized for high throughput and moderate spectral resolution may offer greater scientific return than extremely high-resolution configurations for this class of observations.

9.5. Implications for Target Selection and Mission Design

The results presented here have direct implications for future ultraviolet-capable space missions. Increasing telescope aperture or exposure time improves SNR only as the square root of photon counts, leading to diminishing returns compared to strategic target selection. Prioritizing nearby, UV-quiet G-type stars may therefore yield more efficient detection opportunities than focusing exclusively on small, cool stars with intrinsically weak ultraviolet emission.

Moreover, the strong dependence of detectability on stellar ultraviolet properties underscores the importance of incorporating realistic stellar UV spectra early in mission planning and feasibility studies. Atmospheric detectability cannot be reliably assessed without accounting for the stellar photon budget, particularly in the ultraviolet where photon noise dominates.

9.6. Context Within Previous Work

Previous studies have demonstrated that Earth-like atmospheres can, in principle, produce detectable ultraviolet absorption signatures under favorable conditions. However, many analyses have focused primarily on atmospheric signal amplitudes or relied on idealized stellar spectra. By contrast, our work explicitly quantifies the relative impact of atmospheric variability and stellar photon statistics within a single, self-consistent framework.

This integrated approach clarifies why strong ultraviolet absorption features do not necessarily translate into detectable signals and provides a transparent explanation for the wide range of detectability estimates reported in the literature. In doing so, our results place earlier studies in a unified physical context and offer a quantitative foundation for future investigations.

10. Conclusions

In this work, we have developed a fully coupled, end-to-end framework for assessing the detectability of Earth-like exoplanet atmospheres using ultraviolet transit spectroscopy. Our approach self-consistently links atmospheric absorption physics, vertical structure, limb geometry, instrumental spectral resolution, observed stellar ultraviolet spectra, and photon-limited noise statistics. This unified treatment allows us to move beyond qualitative detectability arguments and to quantitatively evaluate the factors that ultimately govern the observability of terrestrial atmospheres in the ultraviolet.

The key novelty of this study lies in explicitly quantifying the relative roles of atmospheric signal amplitude and stellar ultraviolet photon flux within a single, physically

consistent modeling pipeline. Unlike previous studies that primarily focused on atmospheric composition or relied on idealized stellar spectra, we use observed and calibrated stellar UV spectra to demonstrate that detectability in the ultraviolet is dominated by stellar photon statistics rather than by variations in atmospheric structure or composition alone.

Our main conclusions can be summarized as follows:

1. Ultraviolet transit spectroscopy of Earth-like planets is fundamentally photon-limited.

   For an Earth analog, atmospheric transit depth variations are typically at the level of 10^{-7}–10^{-6}, even in wavelength regions dominated by strong ozone and oxygen absorption. As a result, photon-counting noise sets the dominant limit on detectability under realistic observing conditions.

2. Stellar ultraviolet properties dominate detectability over atmospheric variability.

   Plausible variations in atmospheric composition and vertical structure modify the effective atmospheric height and transit signal by less than an order of magnitude, whereas stellar ultraviolet photon fluxes vary by several orders of magnitude across spectral types and between individual stars. Consequently, stellar properties overwhelmingly control the achievable signal-to-noise ratio in the ultraviolet.

3. Nearby, quiet G-type stars represent the most favorable targets for UV atmospheric characterization of terrestrial exoplanets.

   Although larger stellar radii reduce the relative transit depth compared to M-dwarfs, the substantially higher and more stable ultraviolet photon flux of Sun-like stars (exemplified by τ Ceti) yields significantly improved signal-to-noise ratios and shorter exposure times under photon-limited conditions.

4. High throughput and target selection are more critical than extreme spectral resolution.

   Our results remain robust even under conservative, broadband ultraviolet observing scenarios. This indicates that photon efficiency and careful target prioritization offer greater gains for detectability than marginal increases in spectral resolution for terrestrial exoplanet atmospheres.

Taken together, these findings imply that ultraviolet atmospheric characterization of Earth-like exoplanets is not primarily limited by atmospheric physics, but by stellar ultraviolet brightness and photon statistics. This conclusion has direct implications for the design and scientific optimization of future UV-capable space missions. Instruments optimized for high throughput and moderate spectral resolution, combined with observing strategies that prioritize nearby, UV-quiet Sun-like stars, are likely to provide the greatest scientific return for the detection and characterization of terrestrial exoplanet atmospheres and potential biosignatures.

By establishing a transparent and quantitative framework that connects atmospheric absorption to photon-limited detectability, this study provides a robust foundation for future feasibility studies and mission planning efforts aimed at exploring Earth-like worlds in the ultraviolet.

References

Anderson, G. P., et al. 1986, *AFGL Atmospheric Constituent Profiles (0–120 km)*, AFGL-TR-86-0110

Bétrémieux, Y., & Kaltenegger, L. 2013, *ApJ*, 772, L31

Bétrémieux, Y., & Kaltenegger, L. 2014, *ApJ*, 791, 7

Brion, J., Chakir, A., Daumont, D., et al. 1993, *J. Atmos. Chem.*, 15, 1

Brown, T. M. 2001, *ApJ*, 553, 1006

Burrows, A., Marley, M., & Sharp, C. M. 1999, *ApJ*, 512, 843

France, K., et al. 2016, *ApJ*, 820, 89

Grenfell, J. L., et al. 2014, *Planetary and Space Science*, 98, 66

Goody, R. M., & Yung, Y. L. 1989, *Atmospheric Radiation*

Kaltenegger, L., & Traub, W. A. 2009, *ApJ*, 698, 519

Kreidberg, L. 2018, *Handbook of Exoplanets*

Lecavelier des Etangs, A., et al. 2008, *A&A*, 481, L83

Lovelock, J. E. 1965, *Nature*, 207, 568

Linsky, J. L., et al. 2014, *ApJ*, 780, 61

Liou, K.-N. 2002, *An Introduction to Atmospheric Radiation*

Madhusudhan, N. 2019, *ARA&A*, 57, 617

Meadows, V. S. 2017, *Astrobiology*, 17, 1022

Minschwaner, K., et al. 1992, *J. Geophys. Res.*, 97, 10103

Seager, S., & Sasselov, D. D. 2000, *ApJ*, 537, 916

Segura, A., et al. 2005, *Astrobiology*, 5, 706